

Article

A ML-Based Wind Speed Prediction Model with Truncated Real-Time Decomposition and Multi-Resolution Data

Hui Feng ^{1,2,3} , Yao Jin ⁴, Shujin Laima ^{1,2,3,*}, Feiyang Han ⁴, Wengchen Xu ⁴ and Zhiqiang Liu ⁴

¹ Key Lab of Smart Prevention and Mitigation for Civil Engineering Disasters of the Ministry of Industry and Information, Harbin Institute of Technology, Harbin 150090, China

² Key Lab of Structures Dynamic Behavior and Control of the Ministry of Education, Harbin Institute of Technology, Harbin 150090, China

³ School of Civil Engineering, Harbin Institute of Technology, Harbin 150090, China

⁴ CCCC Highway Consultants Co., Ltd., Beijing 100088, China

* Correspondence: laimashujin@hit.edu.cn

Abstract: Accurate wind speed prediction is of importance for long-span cross-sea bridges. To this end, data decomposition techniques are usually employed to promote accuracy of the prediction model. Since wind speed data come sequentially, real-time decomposition should be adopted. However, real-time decomposition may degrade the accuracy due to the end effect. In this paper, a novel scheme of real-time decomposition that is a combination of truncated real-time decomposition and multi-resolution data is developed. Specifically, truncated real-time decomposition firstly denoises the data and eliminates the end effect; high-resolution data are then introduced to compensate for the information loss. Further, a novel wind speed prediction model that consists of the proposed scheme and neural networks is proposed. Specifically, two gated recurrent unit neural networks are employed to extract features from the obtained original-resolution and high-resolution data, respectively, and a multi-layer perceptron is adopted to utilize extracted features and make predictions. The proposed model is validated on the monitoring wind speed data of two long-span cross-sea bridges. Specifically, the mean absolute error and the root of mean square error of the proposed model on the two datasets are 0.334, 0.445 and 0.233 and 0.316 m/s, which are smaller than benchmark models and demonstrate superiority of the proposed model.

Keywords: wind speed prediction; data decomposition; multi-resolution data; machine learning; long-span bridge



Citation: Feng, H.; Jin, Y.; Laima, S.; Han, F.; Xu, W.; Liu, Z. A ML-Based Wind Speed Prediction Model with Truncated Real-Time Decomposition and Multi-Resolution Data. *Appl. Sci.* **2022**, *12*, 9610. <https://doi.org/10.3390/app12199610>

Academic Editors: José António Correia and Elsa Caetano

Received: 24 August 2022

Accepted: 21 September 2022

Published: 24 September 2022

Publisher's Note: MDPI stays neutral with regard to jurisdictional claims in published maps and institutional affiliations.



Copyright: © 2022 by the authors. Licensee MDPI, Basel, Switzerland. This article is an open access article distributed under the terms and conditions of the Creative Commons Attribution (CC BY) license (<https://creativecommons.org/licenses/by/4.0/>).

1. Introduction

Cross-sea bridges that connect different regions are becoming a more and more important part of the modern transportation network. With cross-sea bridges being longer and lighter, they are more susceptible to wind load. Under strong winds, the serviceability of a long-span cross-sea bridge can be influenced, and there may even be traffic accidents [1–3]. Therefore, there is an urgent need to establish a reliable wind speed prediction model to predict wind speed near the bridge and then aid in the management of the bridge.

A wind speed prediction model can be mainly classified into physics-driven models and data-driven models. Physics-driven models collect related meteorological parameters and employ numeric weather prediction (NWP) models to make wind speed predictions, which require many computing resources and are more suitable for long-term predictions. In addition, post-processing techniques are usually needed for physics-driven models to make wind speed predictions for a specific location [4–6]. Data-driven models predict wind speed by modeling evolutionary mechanisms of wind speed embedded in historical data. As a comparison, data-driven models require fewer computing resources and are more suitable for short-term wind speed prediction for a specific location. According to the

mentioned comparison, data-driven models are more suitable for short-term wind speed prediction for long-span cross-sea bridges.

Traditional data-driven models are time series models, such as the autoregressive moving average (ARMA) model [7] and fractional autoregressive integrated moving average (f-ARIMA) model [8]. Time series models mainly focus on linear characteristics in the historical wind speed data. In order to take nonlinear characteristics into consideration more efficiently, machine learning models such as support vector machine [9], multi-layer perceptron [10] and extreme learning machine [11] were adopted. With the increase in the volume of data and the development of data mining techniques, deep learning models were also applied to predicting wind speed, which can extract multi-level features more efficiently than shallow models. Typical examples are the long short-term memory (LSTM) neural network [12], convolutional neural network (CNN) [13] and deep reinforcement learning model [14].

The accuracy of a data-driven model is easily influenced by the unpredictable noise contained in the historical data. To alleviate the degradation of accuracy caused by the noise, researchers proposed to combine the data decomposition technique with the prediction model. The basic idea is as follows. The raw wind speed series is firstly decomposed into several subseries that are easier to predict. Then, the prediction model is established for each subseries, and the final prediction is made by aggregating the predictions for each subseries. For example, Liu et al. [15] proposed a prediction model with empirical mode decomposition (EMD) and ARIMA. Yu et al. [16] came up with a prediction model with wavelet packet decomposition (WPD) and the Elman neural network (ENN). Liu et al. [17] used singular spectrum analysis (SSA) to decompose the wind speed data and adopted a convolutional neural network gated recurrent unit (CNNGRU) and support vector regression (SVR) to predict the trend and detail components, respectively. Other signal processing techniques such as wavelet transform (WT) [18] and variational mode decomposition (VMD) [19] were also employed. To further enhance the predictability of a subseries, a secondary decomposition is needed. Qu et al. [20] firstly used complete ensemble empirical mode decomposition with adaptive noise (CEEMDAN) to decompose the raw series and then used empirical wavelet transform (EWT) to decompose a subseries of high frequency. Zhang et al. [21] employed VMD to decompose the raw series and then applied WT to denoise each subseries. To decrease computing resources demanded by building a prediction model for each series, researchers proposed several approaches. One approach is to assemble a subseries according to sample entropy [22] or the Spearman correlation coefficient [23]. Another approach is to predict the trend only [24–26]. Researchers also employed a scheme of weighted sums to tackle the problem of error accumulation that occurs when aggregating predictions of each subseries [27,28].

It is effective to combine the signal processing technique and the prediction model to improve accuracy. However, in most related research studies, the signal decomposition was performed at once, which is called one-time decomposition [29] and is based on the assumption that all data are known. However, in practice, wind speed data come sequentially, which indicate the impracticability of one-time decomposition and require real-time decomposition. Real-time decomposition means that data decomposition is performed every time new data come in. The main problem of real-time decomposition is the end effect. The end effect is manifested as the difference between the end region of decomposition results of the initial series and that of the series updated with new wind speed data. The end effect is caused by the difference between endpoint values of these two series. The influence of the end effect on the prediction model is illustrated as follows. For example, a prediction of the trend of wind speed is needed, and trends obtained by decomposition of the updated series r_1, \dots, r_{N+1} and the initial series r_1, \dots, r_N are denoted as t_1^u, \dots, t_{N+1}^u and t_1^i, \dots, t_N^i , respectively. The ideal input should be t_1^u, \dots, t_N^u that is more consistent with the target t_{N+1}^u , but the available input is t_1^i, \dots, t_N^i . There is a difference between the ideal and the available input due to the end effect, which can be interpreted as the introduction of a kind of noise that is caused by the end effect. As a consequence, the

end effect can degrade the improvement of accuracy by data decomposition techniques. The accuracy of the prediction model with this basic real-time decomposition can even be worse than that of the prediction model without signal processing techniques [30,31]. It was suggested to adopt data decomposition techniques as tools of denoising [31], by which only insignificant changes in the raw series are made, and the end effect can be mitigated. How to further reduce the influence of the end effect has become an important topic.

A possible solution is to adopt a new scheme of real-time decomposition that can mitigate end effect. Deng et al. [32] proposed a new scheme of real-time decomposition that is called quasi real-time decomposition, and the scheme is explained as follow. An initial prediction of the raw series is firstly made and supplemented to the raw series, and the updated series is then decomposed to obtain a corresponding subseries, by which the end effect can be mitigated. However, the effectiveness of quasi real-time decomposition depends on the accuracy of the initial prediction. Liu and wang [33] proposed a scheme of real-time decomposition to eliminate the influence of the end effect by discarding the influenced part of the result of decomposition and using the rest as input, which can be regarded as truncated real-time decomposition. Compared to basic real-time decomposition and quasi real-time decomposition, truncated real-time decomposition can eliminate the influence of the end effect explicitly, but it can lose information significantly and transform a single-step prediction problem into a multi-step prediction problem. Thus, the scheme of truncated real-time decomposition requires auxiliary measures.

Recently, researchers studied the possibility of applying multi-resolution data to wind speed prediction. Wang et al. [34] used low-resolution and high-resolution data as the input of the functional regression model to enhance its ability to capture patterns of different time scales. Wang et al. [35] applied the kernel-based ELM (KELM) to combine predictions by a model trained using low-resolution data and by a model trained using high-resolution data. In the aforementioned studies, the introduction of high-resolution data can provide details of wind speed series and improve the accuracy. Therefore, it is possible to combine truncated real-time decomposition and multi-resolution data to mitigate the influence of end effect without losing information significantly.

In this paper, we propose multi-resolution real-time decomposition, which is a new scheme of real-time decomposition that combines truncated real-time decomposition and multi-resolution data. Furthermore, we propose a wind speed prediction model with the proposed scheme and GRU neural networks and term the proposed model as SSA-TRTD-MR-GRU. Specifically, the proposed scheme consists of two parts. One is to denoise the original series with the scheme of truncated real-time decomposition. The other is to collect the high-resolution data to compensate for the information loss caused by truncated real-time decomposition. The proposed model is composed of two GRU neural networks and one MLP. In the proposed model, two GRU neural networks are used to extract features from the original-resolution input and the high-resolution input, respectively, and the MLP is used to take extracted features as input and make the prediction. The comparison of the proposed model with relevant research studies is summarized in Table 1. The proposed model is validated with monitoring wind speed data in the site of two long-span cross-sea bridges.

The proposed scheme connects truncated real-time decomposition with multi-resolution data, which extend real-time decomposition techniques. Furthermore, the proposed model connects the proposed scheme with deep learning techniques, which can make more accurate predictions. The remainder of this paper is as follows. In Section 2, the theoretical background of the SSA and GRU neural network, schemes of real-time decomposition are introduced, and the details of the proposed scheme and model are given. Section 3 introduces the data description and the parameter setting of SSA. Analyses of the experimental results and the conclusion are provided in Sections 4 and 5, respectively.

Table 1. The comparison of the proposed model with relevant research studies.

Ref	Method	Real-Time Decomposition	Multi-Resolution Data
[15]	EMD + ARIMA	No	No
[16]	WPD + ENN	No	No
[17]	SSA + CNNGRU + SVR	No	No
[20]	CEEMDAN + EWT + NN	No	No
[21]	VMD + WT + RBF	No	No
[24]	MCEEMDAN + QRNN	No	No
[25]	CEEMD + ARMA + BPNN	No	No
[26]	WTD + GRU	No	No
[27]	VMD + SVM + LSTM	No	No
[28]	VMD + RBF	No	No
[31]	EMD + SVM	Basic real-time decomposition	No
[32]	EWT + ENN	Quasi real-time decomposition	No
[33]	SSA + BiLSTM	Truncated real-time decomposition	No
[34]	Functional regression	No	Yes
[35]	ICEEMDAN	No	Yes
Proposed	SSA + GRU	Truncated real-time decomposition	Yes

2. Methodology

2.1. SSA

Singular spectrum analysis (SSA) is a non-parametric method that is usually used to extract trends from nonlinear and noisy time series [36,37]. SSA has the advantage that only a small part of the extracted trend is significantly influenced by the end effects. Furthermore, the length of the influenced part is fixed and closely relevant to the window length of SSA [33]. To this end, SSA is selected as the data decomposition technique in this paper.

Given the wind speed series $\mathbf{x}_i = (x_1, \dots, x_N)$ of length N , window length L , $K = N - L + 1$ and grouping parameter r , the main procedure of SSA to denoise the series is as follows [38]. SSA consists of the decomposition stage and the reconstruction stage. In the decomposition stage, the original series is firstly transformed into the trajectory matrix \mathbf{X} by embedding, which is shown in Equations (1) and (2):

$$\mathbf{X} = [\mathbf{x}_1 \quad \dots \quad \mathbf{x}_K] = \begin{bmatrix} x_1 & \dots & x_k \\ \vdots & \ddots & \vdots \\ x_L & \dots & x_N \end{bmatrix} \tag{1}$$

$$\mathbf{x}_i = (x_i, \dots, x_{i+L-1})^T \tag{2}$$

in which \mathbf{x}_i is called the lagged vector. The trajectory is then decomposed by the singular value decomposition (SVD). With the obtained eigen-triples $(\sqrt{\lambda_i}, \mathbf{u}_i, \mathbf{v}_i)$ ($\sqrt{\lambda_i}$ is the singular value of the i th eigen-triple, \mathbf{u}_i denotes the corresponding eigenvector and $\mathbf{v}_i = \mathbf{X}^T \mathbf{u}_i / \sqrt{\lambda_i}$) of the SVD, the trajectory matrix can be rewritten as follow:

$$\mathbf{X} = \mathbf{X}_1 + \dots + \mathbf{X}_d \tag{3}$$

where $\mathbf{X}_i = \sqrt{\lambda_i} \mathbf{u}_i \mathbf{v}_i^T$ is called the elementary matrix, and d is the number of eigen-triples. In the reconstruction stage, eigen-triple grouping is firstly performed to select eigen-triples and their corresponding elementary matrices, which is to choose r eigen-triples of all d eigen-triples and construct the trajectory matrix of the trend by these elementary matrices. The grouping can be expressed as:

$$\mathbf{X}_{trend} = \mathbf{X}_1 + \dots + \mathbf{X}_r \tag{4}$$

where X_{trend} is the trajectory matrix of the trend of the original series. Finally, the diagonal averaging is performed to transform X_{trend} to the trend x_{trend} of the original series. The diagonal averaging is given as follows (Y is used to denote X_{trend} for simplicity):

$$y_j = \begin{cases} \frac{1}{j} \sum_{i=1}^j Y_{i,j-i+1}, 1 \leq j < L \\ \frac{1}{L} \sum_{i=1}^L Y_{i,j-i+1}, L \leq j < K \\ \frac{1}{N-j+1} \sum_{i=j-K+1}^{N-K+1} Y_{i,j-i+1}, K \leq j \leq N \end{cases} \quad (5)$$

in which y_j is j th element of x_{trend} .

The performance of SSA is controlled by the window length and the grouping parameter r . The grouping parameter can be selected by inspecting the eigenvalue spectrum, and the window length can be selected by comparing results of denoising [39].

2.2. GRU

Recurrent neural network (RNN) is popular in wind speed prediction for its capacity of extracting features from sequences. Gated recurrent unit (GRU) is a modification of the naïve RNN cell, which introduces the update gate and the reset gate to control the information flow and then tackle the problem of gradient vanishing [40–43]. Therefore, GRU is chosen to be the model to extract features of wind speed series. The typical GRU neural network for wind speed prediction is shown in Figure 1a, where x_i , h_i , GRU and FC denote i th input, i th hidden state, GRU cell and fully connected layer (single-hidden-layer neural network), respectively. As shown in Figure 1a, the GRU cell is used to process the input sequence and store extracted features in the final hidden state, which is the input of a fully connected layer to make the prediction.

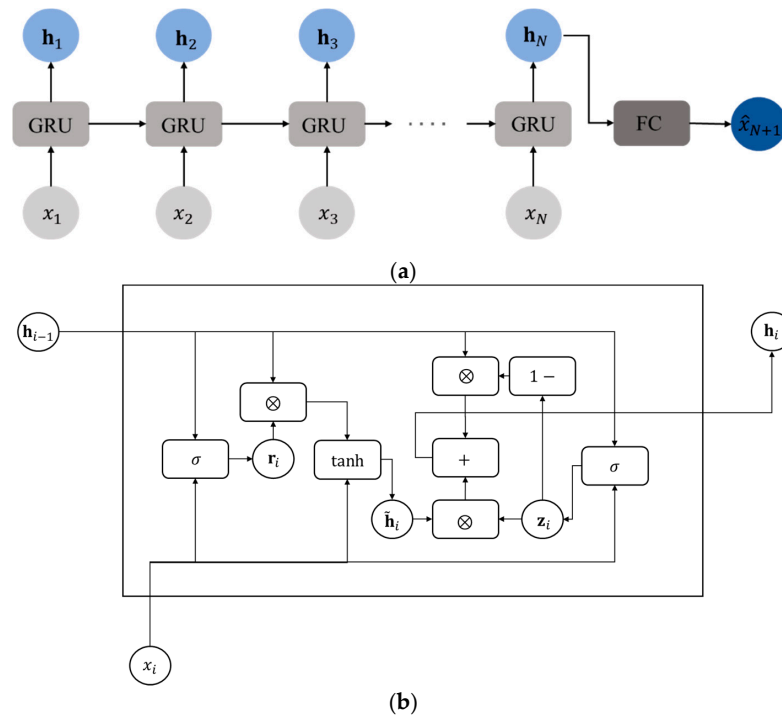


Figure 1. The schematic diagram of GRU neural network and its cell: (a) typical GRU neural network; (b) schematic diagram of GRU neural network and its cell.

The structure of the GRU cell is shown in Figure 1b, where $\mathbf{r}_i, \mathbf{z}_i, \tilde{\mathbf{h}}_i, \otimes, \tanh, \sigma$ denote reset gate, update gate, candidate hidden state, element-wise multiplication, hyperbolic tangent function, and sigmoid function, respectively. The information flow inside the cell can be written as follows [40]:

$$\mathbf{r}_i = \sigma(\mathbf{W}_{rh}\mathbf{h}_{i-1} + \mathbf{W}_{rx}x_i + \mathbf{b}_r) \tag{6}$$

$$\mathbf{z}_i = \sigma(\mathbf{W}_{zh}\mathbf{h}_{i-1} + \mathbf{W}_{zx}x_i + \mathbf{b}_z) \tag{7}$$

$$\tilde{\mathbf{h}}_i = \tanh(\mathbf{W}_{hh}(\mathbf{r}_i \otimes \mathbf{h}_{i-1}) + \mathbf{W}_{hx}x_i + \mathbf{b}_h) \tag{8}$$

$$\mathbf{h}_i = \mathbf{z}_i \otimes \tilde{\mathbf{h}}_i + (1 - \mathbf{z}_i) \otimes \mathbf{h}_{i-1} \tag{9}$$

in which $\mathbf{W}_{rh}, \mathbf{W}_{rx}, \mathbf{W}_{zh}, \mathbf{W}_{zx}, \mathbf{W}_{hh}, \mathbf{W}_{hx}$ are the weights and $\mathbf{b}_r, \mathbf{b}_z, \mathbf{b}_h$ are the biases.

2.3. Schemes of Real-Time Decomposition

Due to the fact that wind speed data come sequentially, real-time decomposition is more suitable than one-time decomposition. There are three schemes of real-time decomposition in the literature, which are basic real-time decomposition [31], quasi real-time decomposition [32] and truncated real-time decomposition [33]. Diagrams of these three schemes are shown in Figure 2, where data in the blue cube denote the data influenced by the end effect (the length of the influenced part is set to be 2 presumably).

As shown in Figure 2a, the trend t_1, \dots, t_N is obtained by denoising the existing series r_1, \dots, r_N using SSA, and it is used as direct input in the scheme of basic real-time decomposition. The scheme of quasi real-time decomposition is shown in Figure 2b. The initial prediction \tilde{r}_{N+1} is made for the existing series to obtain an extended series $r_1, \dots, r_N, \tilde{r}_{N+1}$. Then, SSA is performed on the extended series to obtain the trend $t_1, \dots, \tilde{t}_N, \tilde{t}_{N+1}$, and the trend is truncated to avoid the introduction of error caused by the initial prediction. Finally, the truncated trend t_1, \dots, \tilde{t}_N is taken as input. In the scheme of truncated real-time decomposition, as shown in Figure 2c, the existing series is processed by SSA to obtain the trend, and the trend is truncated to discard the data influenced by the end effect. The truncated trend t_1, \dots, t_{N-2} is then used as input.

Both the input obtained using basic real-time decomposition and quasi real-time decomposition are influenced by the end effect. Quasi real-time decomposition can mitigate the end effect by making the obtained trend closer to the ideal trend that is obtained by processing the series that is updated with true oncoming wind speed data. However, the effectiveness of quasi real-time real data relies on the accuracy of the initial prediction.

Furthermore, truncated real-time decomposition eliminates the influenced data explicitly. However, truncated real-time decomposition also eliminates the latest data that contain the most recent information, which can transform a single-step prediction problem into a multi-step prediction problem and thus decrease the accuracy.

2.4. SSA-TRTD-MR-GRU

The proposed scheme of real-time decomposition and the proposed model of wind speed prediction are shown in Figure 3.

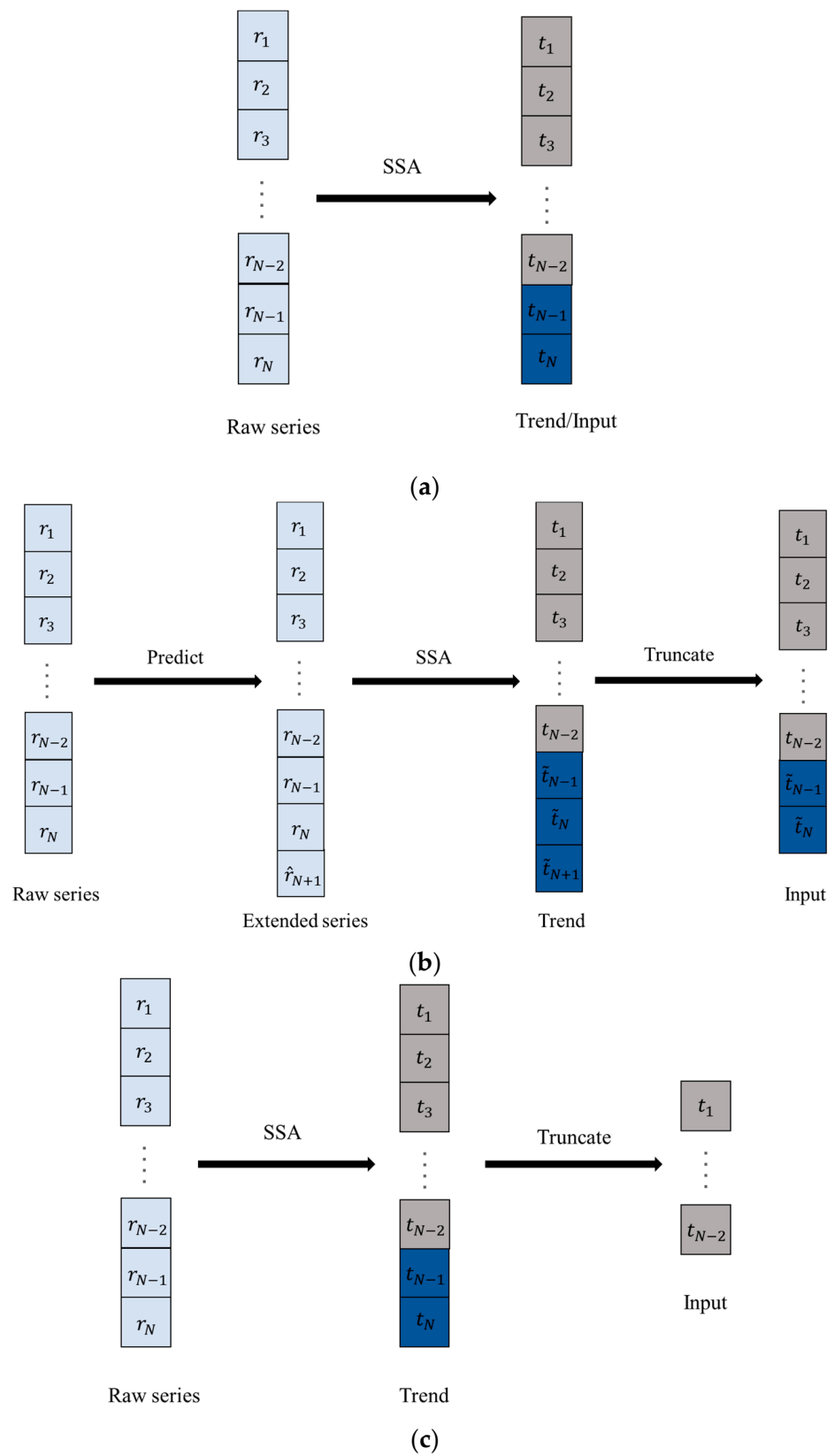


Figure 2. Diagrams of three schemes of real-time decomposition: (a) basic real-time decomposition; (b) quasi real-time decomposition; (c) truncated real-time decomposition.

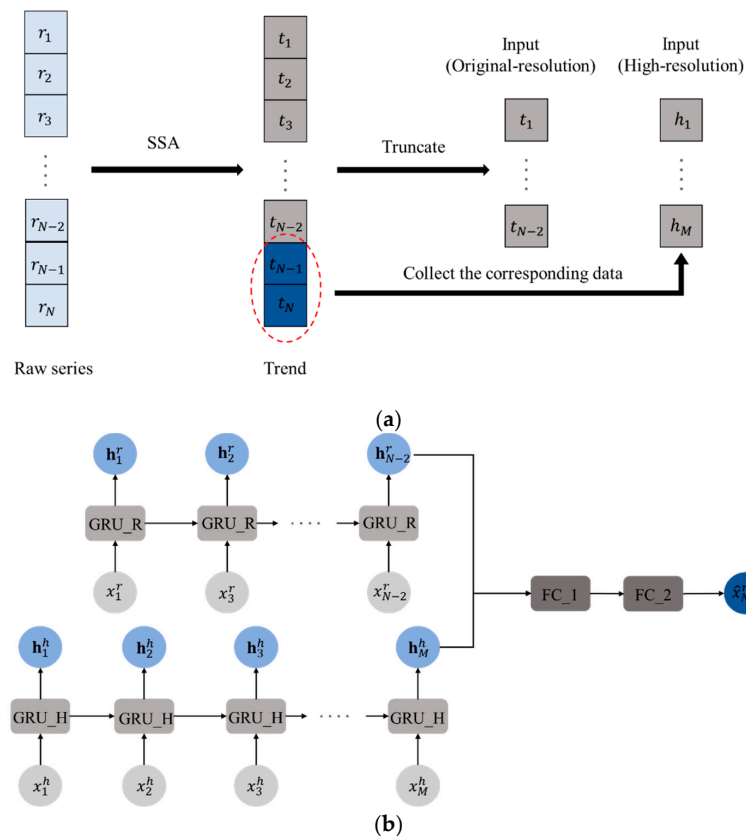


Figure 3. Diagrams of the proposed scheme and model: (a) multi-resolution real-time decomposition; (b) SSA-TRTD-MR-GRU.

As shown in Figure 3a, the proposed scheme consists of two parts. In the first part, truncated real-time decomposition is performed to obtain the truncated trend as the input of original resolution. In the second part, the corresponding high-resolution data are collected as the input of high resolution to compensate for the information loss during performing truncated real-time decomposition. To illustrate, time intervals of the original-resolution and the high-resolution data are set to 10 and 1 min, respectively, and lengths of the trend (without truncated) and its influenced part are set to 12 and 2, respectively. After the first part, the truncated trend t_1, \dots, t_{N-2} is used as the input of original resolution with the loss of the information at about t_{N-1}, t_N . To compensate for the information loss of the trend of the most recent 20 min, the corresponding high-resolution data h_1, \dots, h_{20} that have time resolution of 1 min are used as the input of high resolution. The proposed scheme is a combination of truncated real-time decomposition and multi-resolution data. With the aid of truncated real-time decomposition, the real-time denoised input can be obtain without introducing the error caused by the end effect. Furthermore, with the aid of the corresponding high-resolution data, the information loss caused by truncated real-time decomposition can be compensated.

As shown in Figure 3b, the proposed model consists of three sub-neural networks. Two GRU networks are used to extract features from the original-resolution input and the high-resolution input, respectively. One MLP is adopted to utilize the extracted features to make a prediction. Specifically, the proposed model is explained as follows. GRU_R denotes the GRU neural network that takes the original-resolution data x_1^r, \dots, x_{N-2}^r as input and the extracted features stored in h_{N-2}^r . GRU_H denotes the GRU neural network that takes the high-resolution data x_1^h, \dots, x_M^h as input and extract features stored in h_M^h . An MLP that consists of two fully connected layers (FC_1 and FC_2) output the prediction x_{N+1}^r by utilizing the hidden state that is concatenated by h_{N-2}^r and h_M^h . The proposed model is a combination of the proposed scheme of real-time decomposition and neural

networks. With the aid of the proposed scheme of real-time decomposition, both the trend and the detail series can be obtained and used as input. With the aid of neural networks, high-level features embedded in the original-resolution and the high-resolution data can be extracted and utilized.

3. Data Description and Decomposition

3.1. Data Description

The proposed scheme and the proposed model are validated on the monitoring wind speed data of two long-span cross-sea bridges. The investigated Bridge A is a cable-stayed bridge with a main span of 392 m, and the investigated Bridge B is a cable-stayed bridge with a main span of 428 m. Both the investigated Bridge A and Bridge B are in Zhejiang province, China, and the locations of these two bridges are shown in Figure 4. Wind speed data of both the investigated Bridge A and Bridge B are measured by three-dimensional ultrasonic anemometers, whose sample frequency are 10 Hz. Data of good integrity and quality are selected for model validation. Specifically, monitoring wind speed data from 1 January to 30 April 2018 are selected for the investigated Bridge A and are denoted as A2018, while monitoring wind speed data from 1 January to 30 April 2019 are selected for the investigated Bridge B and are denoted as B2019. The raw monitoring wind speed is transformed into the 10 min average wind speed data (original-resolution data) and the 1 min average wind speed data (high-resolution data) for both bridges. Time history plots of 10 min average wind speed data of A2018 and B2019 are shown in Figure 5, and corresponding descriptive statistics are summarized in Table 2.

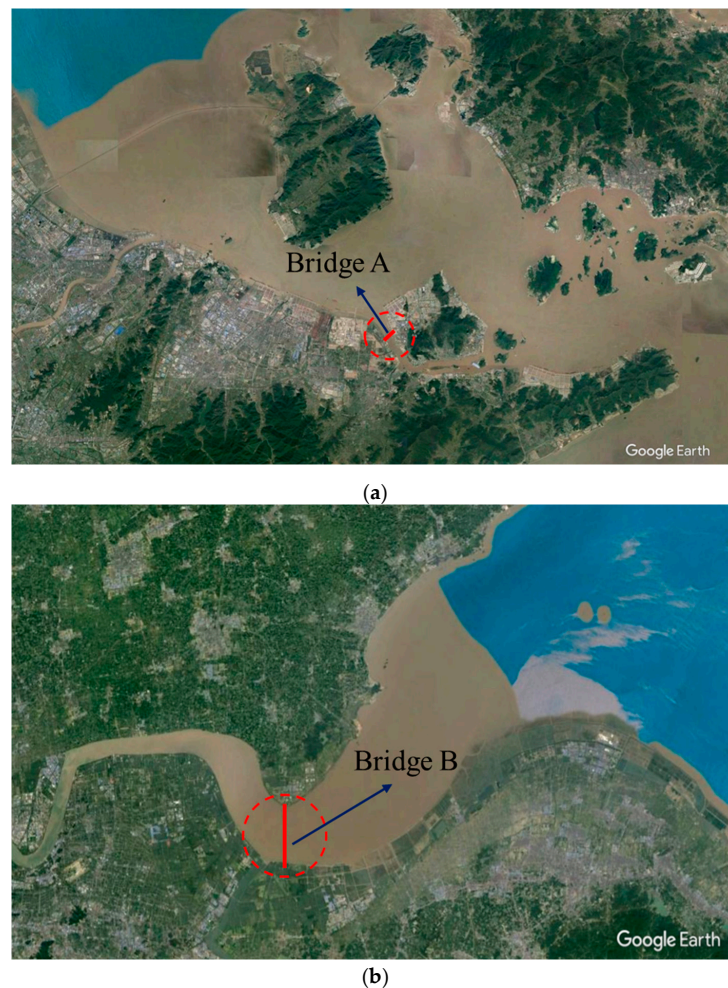


Figure 4. Locations of the investigated Bridge A and Bridge B: (a) Bridge A; (b) Bridge B.

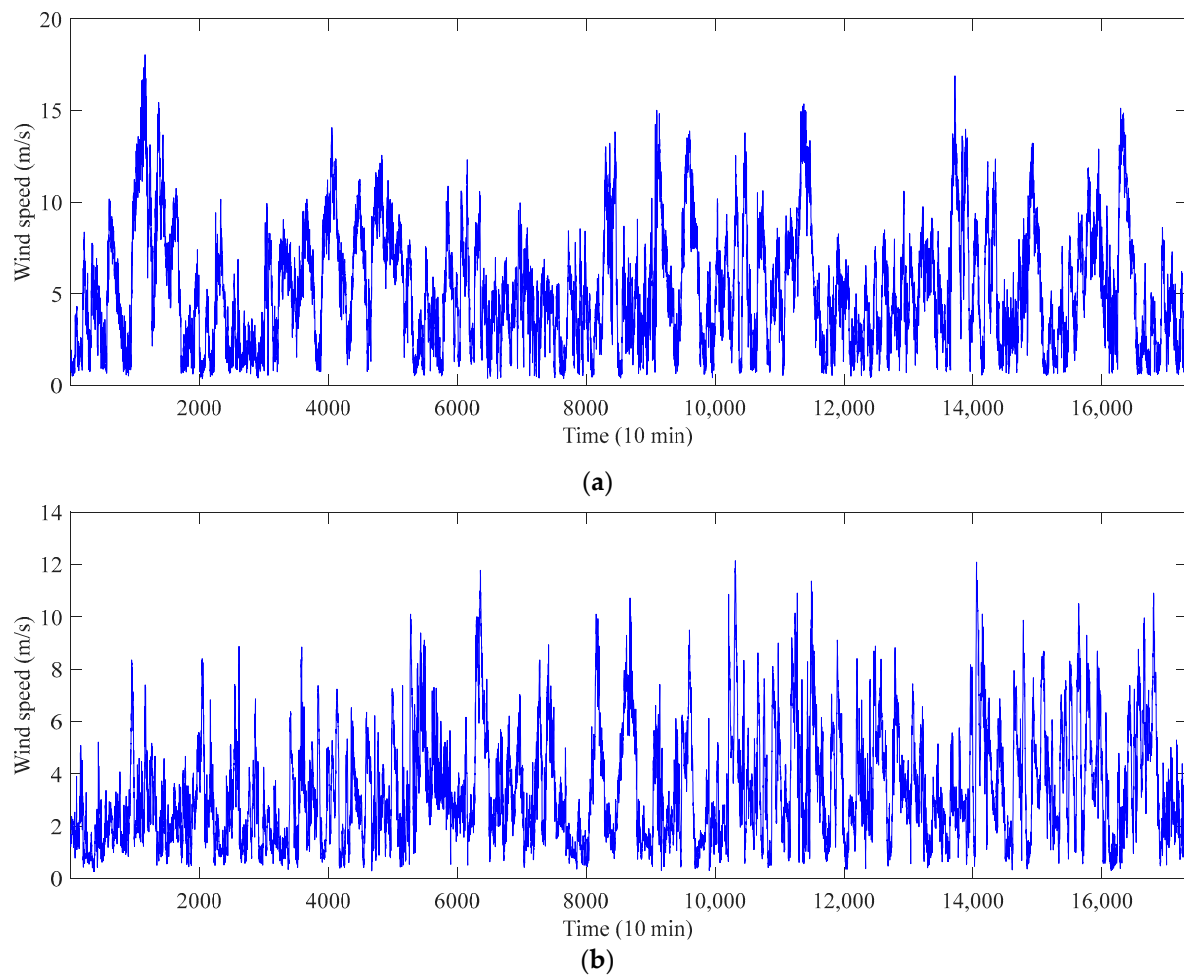


Figure 5. Time history plots of 10 min average wind speed data of the A2018 and B2019: (a) A2018; (b) B2019.

Table 2. Descriptive statistics of 10 min average wind speed data of the A2018 and B2019.

Dataset	Maximum (m/s)	Mean (m/s)	Minimum (m/s)	Standard Deviation (m/s)	Skewness	Kurtosis
A2018	18.04	5.21	0.38	3.21	2.96	0.70
B2019	12.14	3.38	0.27	2.12	3.47	0.95

As shown in Figure 5, both A2018 and B2019 contain significant fluctuations. As shown in Table 2, A2018 and B2019 are of different characteristics. The maximum 10 min average wind speed of A2018 is 18.04 m/s and that of B2019 is 12.14 m/s, which are both above 10 m/s and can influence the serviceability of bridges. Both the maximum and mean wind speed of A2018 are larger than those of B2019. The standard deviation of A2018 is 3.21 m/s, which is also larger than that of B2019 and indicates fluctuations of A2018 are more significant. In addition, skewness and kurtosis of A2018 and B2019 indicate that distributions of 10 min average wind speed of A2018 and B2019 are deviated from Gaussian distribution.

3.2. Data Decomposition

SSA is adopted to perform real-time decomposition, and the parameter settings of SSA of A2018 are presented as an example and are as follows. The parameters of SSA are the window length L and the grouping parameter r . In this paper, the grouping parameter is

determined by comparing eigenvalue spectra, and the window length is determined by comparing results of denoising and influences of the end effect.

The grouping parameter needs to be determined firstly for subsequent analysis, and eigenvalue spectra of different window lengths are shown in Figure 6. As shown in Figure 6, the first eigenvalue plays a dominant role in all the eigenvalue spectra, and the remaining eigenvalues are similarly small. This phenomenon indicates that the first eigen-triplet corresponds to the trend of the series and the remaining eigen-triplets correspond to noises for all the eigenvalue spectra, according to the assumption that the trend is the main component of the series, and the relative contribution to the series can be assessed by the relative value of the eigenvalue. As a consequence, the grouping parameter r is set to 1.

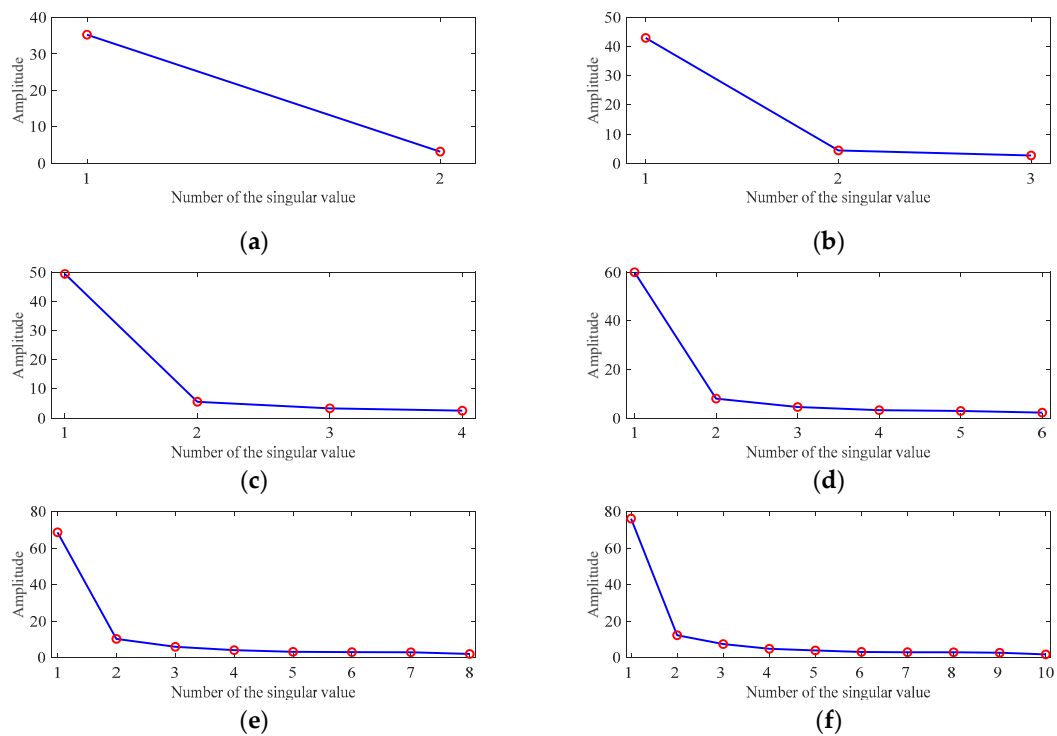


Figure 6. Eigenvalue spectra of different window lengths: (a) $L = 2$; (b) $L = 3$; (c) $L = 4$; (d) $L = 6$; (e) $L = 8$; (f) $L = 10$.

The results of denoising of different window length are then compared, and the results are shown in Figure 7. As shown in Figure 7, SSA of different window lengths can denoise the raw series to varying degrees with the grouping parameter being 1, and the SSA of window lengths larger than 6 produces similar denoised trends. SSA of small window lengths, such as 2, tends to preserve more fluctuations, which can still contain unpredictable noise. Furthermore, SSA of large a window length, such as 8, tends to extract a smoother trend, which is easier to predict.

The choice of window length also needs to take the end effect into consideration, and the end effects of different window length are shown in Figure 8. As shown in Figure 8, the influence range of the end effect increases with the increase in window length. To avoid the large computation caused by the introduction of long high-resolution series to compensate for the information loss, the influence range of the end effect should be kept at a small length. As a consequence, window length should be as small as possible. There exists a trade-off between the denoising performance and the influencing range of the end effect. The window length is set to 3 to obtain a satisfactory denoising performance with a small influence range of the end effect. In summary, the window length is set to 3 and the grouping parameter is set to 1, and the length of the corresponding range of the end effect is 2. The same conclusion can be drawn for B2019.

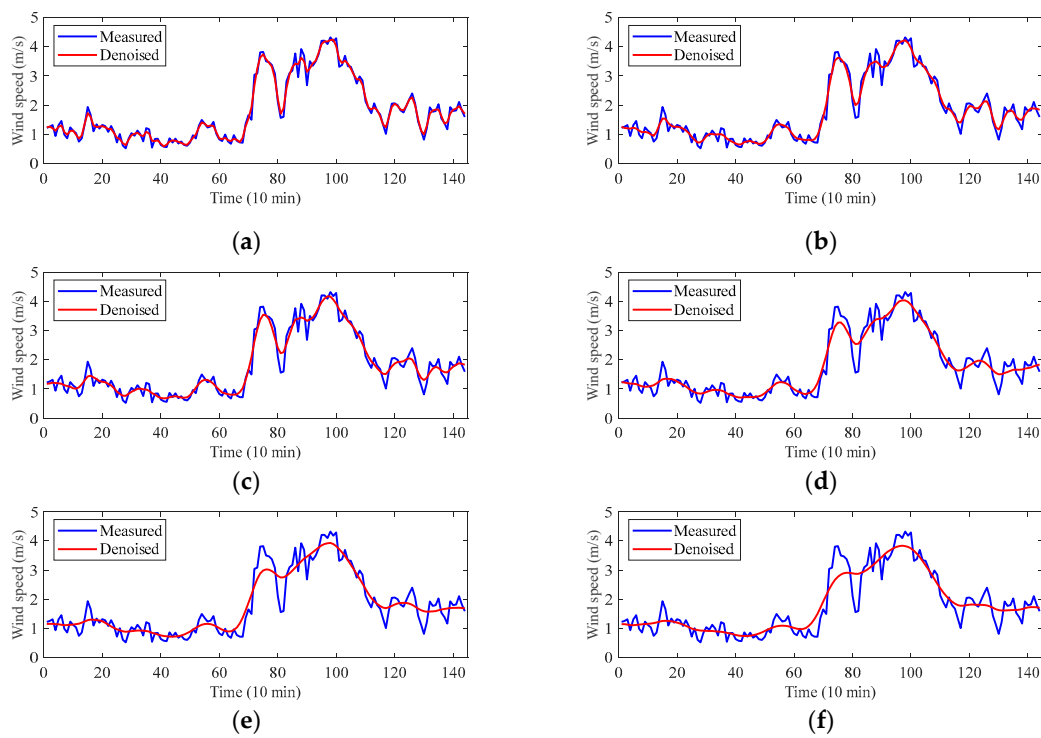


Figure 7. Results of denoising of different window lengths: (a) $L = 2$; (b) $L = 3$; (c) $L = 4$; (d) $L = 6$; (e) $L = 8$; (f) $L = 10$.

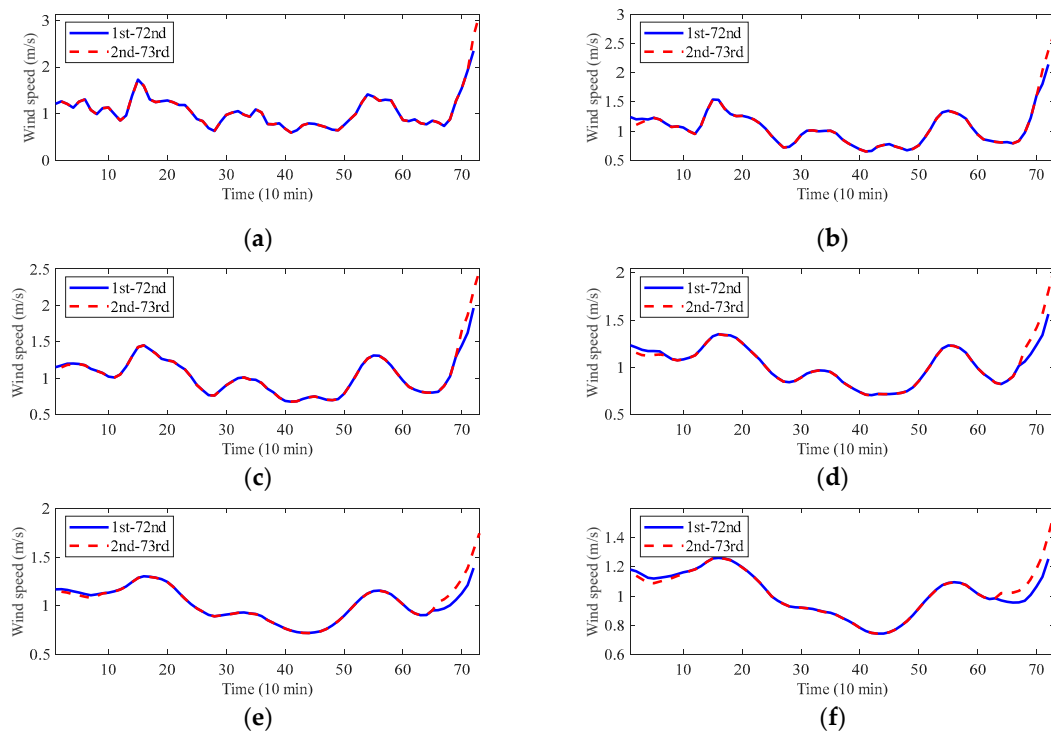


Figure 8. End effects of different window lengths: (a) $L = 2$; (b) $L = 3$; (c) $L = 4$; (d) $L = 6$; (e) $L = 8$; (f) $L = 10$.

4. Experimental Results and Analysis

An experiment is designed to illustrate the superiority of the proposed model, and two kinds of models are included. The first kind of model utilizes the raw existing data to predict the raw wind speed in the future, and the included models are the persistence model

(a naïve model that uses the latest observation as the prediction), ARIMA, extreme learning machine [44–46], CNN [47,48] and GRU neural networks. The second kind of models are GRU neural networks combined with different schemes of real-time decomposition to obtain the denoised input and to predict the trend of the wind speed in the future. The aforementioned models are summarized in Table 3.

Table 3. The summary of models.

Model	Definition
PM	Persistence model
ARIMA	Autoregression integrated moving average model
ELM	Extreme learning machine
CNN	Convolution neural network
GRU	Gated recurrent unit neural network
SSA-BRTD-GRU	GRU with basic real-time decomposition
SSA-QRTD-GRU	GRU with quasi real-time decomposition
SSA-TRTD-GRU	GRU with truncated real-time decomposition
SSA-TRTD-MR-GRU	The proposed model: GRU with real-time decomposition and multi-resolution data

The first four-fifths of the dataset is used to train the models and the remaining one-fifth is used to test the models for both A2018 and B2019. Single-step prediction is performed as an example for all the models to reveal their effectiveness. Specifically, the twelve latest 10 min average wind speed data are used to predict the next 10 min average wind speed data for the first kind of models, and the extracted trend of the twelve latest 10 min average wind speed data by different schemes of real-time decomposition is used to predict the next wind speed data of the trend. As for truncated real-time decomposition and the high-resolution data, the latest two wind speed data of the extracted trend are discarded, and the corresponding twenty latest 1 min average wind speed data are used as the compensating high-resolution data.

4.1. Evaluation Metrics

The mean absolute error (MAE) and the root square mean error (RMSE) that can reflect the difference in the actual value and the prediction value are adopted to evaluate the performance of the prediction model. The formulas of the MAE and RMSE are shown in Equations (10) and (11).

$$\text{MAE} = \frac{1}{N} \sum_{i=1}^N |z_i - \hat{z}_i| \quad (10)$$

$$\text{RMSE} = \sqrt{\frac{1}{N} \sum_{i=1}^N (z_i - \hat{z}_i)^2} \quad (11)$$

where z_i is i th actual value and \hat{z}_i is i th prediction, and N is the number of predictions. The mean absolute percentage error (MAPE) is not adopted because a large proportion of the wind speed data is small, and small absolute error of the prediction can lead to large an absolute percentage error, which can hinder the analysis of the performance of the prediction model.

4.2. Experimental Results

Typical predictions of the proposed model are shown in Figure 9, and the performance of the aforementioned models on the testing set of A2018 and B2019 are summarized in Table 4. As shown in Figure 9, the proposed model can make satisfactory predictions of the trend of wind speed. As shown in Table 4, the proposed model achieved the highest accuracy on both the testing sets of A2018 and B2019, which indicates superiority of the

proposed method. To illustrate, the MAE and RMSE of the proposed model on the testing set of A2018 are significantly smaller than those of other models. Two detailed analyses are conducted to reveal the effectiveness of the proposed model, which are presented in Sections 4.3 and 4.4.

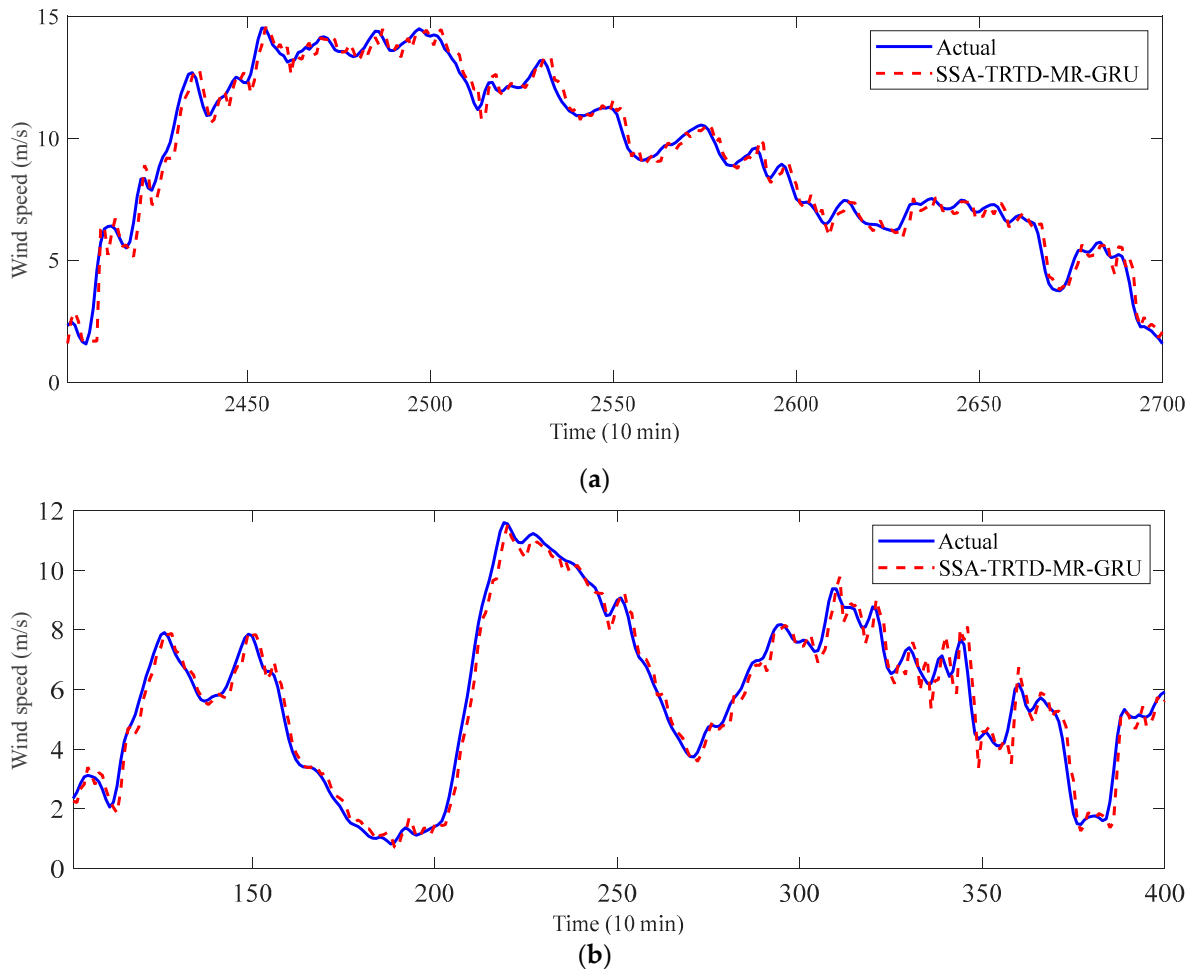


Figure 9. Typical prediction of testing sets of A2018 and B2019 by the proposed model: (a) A2018; (b) B2019.

Table 4. The summary of prediction accuracies of models.

	A2018		B2019	
	MAE (m/s)	RMSE (m/s)	MAE (m/s)	RMSE (m/s)
PM	0.503	0.676	0.310	0.434
ARIMA	0.501	0.670	0.308	0.429
ELM	0.501	0.669	0.309	0.431
CNN	0.499	0.669	0.309	0.429
GRU	0.499	0.667	0.307	0.428
SSA-BRTD-GRU	0.391	0.518	0.270	0.364
SSA-QRTD-GRU	0.372	0.494	0.261	0.353
SSA-TRTD-GRU	0.431	0.567	0.306	0.413
SSA-TRTD-MR-GRU	0.334	0.445	0.233	0.316

4.3. Analysis I: The Performance of Data Decomposition

A comparison between the models without data composition and the proposed model is conducted to analyze the effectiveness of the data composition. The comparison is shown in Figure 10, and several discoveries can be made as follows.

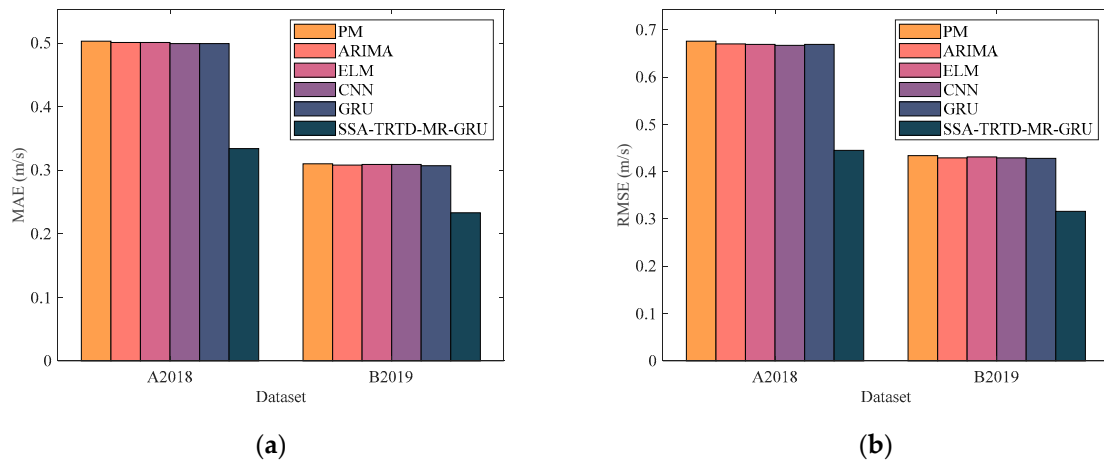


Figure 10. The comparison between the models without data composition and the proposed model: (a) MAE; (b) RMSE.

Firstly, as shown in Figure 10 and Table 4, the PM model has the worst accuracy and the GRU model has the best accuracy among the models without data decomposition. However, differences between their accuracies are insignificant. To illustrate, the MAE and RMSE of PM that has the worst accuracy on the testing set of A2018 are 0.503 and 0.676 m/s, respectively, while those of GRU are 0.499 and 0.667 m/s. The accuracy of GRU is not significantly higher than that of PM. The reason behind this is the phenomenon of unpredictable noise embedding in the raw wind speed series, which can mask the characteristics of wind speed and then prevent the models from learning evolution patterns of wind speed. As a consequence of this discovery, PM is used to make initial predictions in the scheme of quasi real-time decomposition for its simplicity.

Secondly, the proposed model with the help of data decomposition can achieve a significantly higher accuracy than the models without data decomposition. For example, the MAE and RMSE of SSA-TRTD-MR-GRU on the testing set of A2018 are 0.334 and 0.445 m/s, respectively, which are significantly smaller than those of GRU. The reason behind this superior performance is that data decomposition can extract the trend of the raw wind speed series and eliminate the unpredictable noise effectively, which makes it easier for the prediction model to learn latent mechanisms. In effect, all the models with data decomposition can have higher accuracy than the models without data decomposition. The aforementioned discoveries can be summarized as follows. GRU can predict the wind speed data more accurately than other models, and data decomposition can promote the accuracy of models.

4.4. Analysis II: The Performance of the Proposed Scheme of Real-Time Decomposition

A comparison between the models with different schemes of real-time decomposition is conducted to analyze the effectiveness of the proposed scheme. The comparison is shown in Figure 11, and several discoveries can be made as follows.

Firstly, it can be seen that SSA-QRTD-GRU has higher accuracy than SSA-BRTD-GRU. For example, the MAE and RMSE of SSA-QRTD-GRU on the testing set of A2018 are 0.372 and 0.494 m/s, respectively, while those of SSA-BRTD-GRU are 0.391 and 0.518 m/s. The reason behind this phenomenon is that the scheme of quasi real-time decomposition can produce an input that is less influenced by the end effect. Secondly, the accuracies of SSA-BRTD-GRU and SSA-QRTD-GRU are higher than that of SSA-TRTD-GRU. For instance, the MAE and RMSE of SSA-TRTD-GRU on the testing set of A2018 are 0.431 and 0.567 m/s, respectively, which is caused by the information loss during the truncation of the extracted trend and indicates the need of supplemental information.

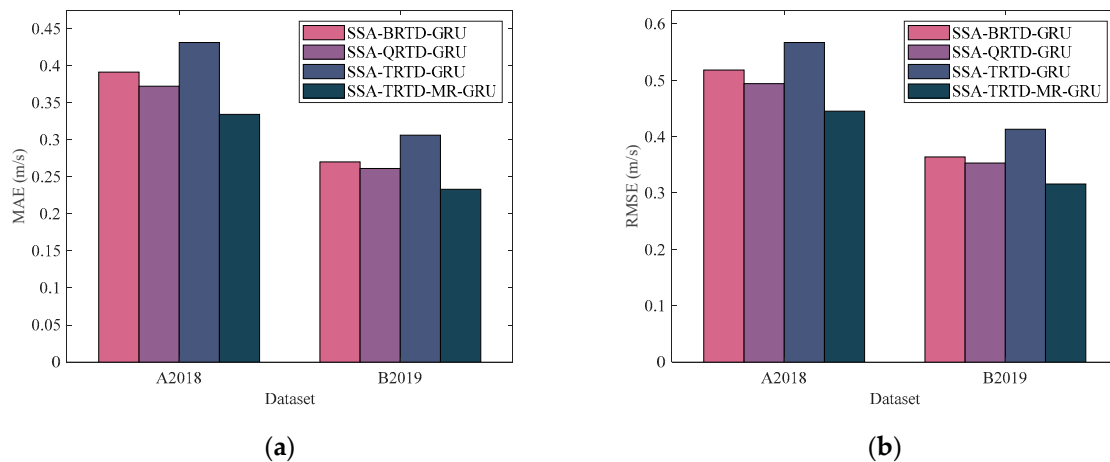


Figure 11. The comparison between the models with different schemes of real-time decomposition: (a) MAE; (b) RMSE.

Thirdly, the proposed model has the highest accuracy among the models with different schemes of real-time decomposition. The reason behind this phenomenon is as follows. The proposed scheme can eliminate the influenced part of input and avoid the noise caused by the end effect, which is superior to basic real-time decomposition and quasi real-time decomposition. Furthermore, the proposed scheme introduces the supplemented high-resolution data to effectively compensate for the information loss, which is superior to truncated real-time decomposition. The aforementioned discoveries can be summarized as follows. The proposed model with the proposed scheme of real-time decomposition can predict the wind speed data more accurately than models with other schemes of real-time decomposition, and the proposed scheme is more effective than other schemes. Compared with the other three schemes of real-time decomposition, the proposed scheme can eliminate the influenced part of the extracted trend explicitly without information loss.

5. Conclusions

In this paper, a new wind speed prediction model with a new scheme of real-time decomposition is proposed to predict wind speed near cross-sea bridges. Specifically, a scheme of real-time decomposition that combines truncated real-time decomposition and multi-resolution is proposed, which discards the part of input influenced by the end effect and collects corresponding high-resolution data to compensate for the information loss. Further, a prediction model that combines the proposed scheme of real-time decomposition and neural networks is proposed, where two gated recurrent unit (GRU) neural networks are used to extract features from multi-resolution data, and a multi-layer perceptron (MLP) is employed to utilize extracted features to make predictions. The proposed model is validated on the monitoring wind speed data of two long-span cross-sea bridges, and the superiority of the model is illustrated through comparisons. The reason for the superiority of the proposed model is as follows. Firstly, the GRU neural network is more suitable for extracting features from time series than from convolutional neural networks (CNN) and shallow models, such as extreme learning machine (ELM). Secondly, data decomposition can enhance the predictability of wind speed by effectively eliminating the unpredictable noise. Thirdly, the proposed scheme is superior to existing schemes of real-time decomposition for its ability to discard the influenced part of input and compensating relevant information. In summary, the proposed scheme provides a new approach to conduct real-time decomposition, and the proposed model can utilize the proposed scheme to make wind speed predictions with higher accuracy.

The major limitation of the proposed model is that only the trend of wind speed is predicted and the uncertainty of wind speed is not considered. The uncertainty of wind speed is mainly reflected in the unpredictable noise, which is eliminated by data

decomposition to promote the prediction accuracy of the model. The quantification of the uncertainty of wind speed by interval prediction or distribution prediction can enhance the reliability of the prediction of the trend. To this end, future work should extend the proposed model to probabilistic prediction and solve this major limitation.

Author Contributions: Conceptualization, H.F. and S.L.; methodology, H.F. and S.L.; software, H.F.; validation, H.F. and S.L.; formal analysis, H.F. and S.L.; investigation, H.F., S.L., Y.J., S.L., F.H. and W.X.; resources, S.L., Y.J., S.L., F.H., W.X. and Z.L.; data curation, H.F.; writing—original draft preparation, H.F. and S.L.; writing—review and editing, H.F. and S.L.; visualization, H.F. and S.L.; supervision, S.L.; project administration, S.L.; funding acquisition, S.L. All authors have read and agreed to the published version of the manuscript.

Funding: This research was funded by Funds for the National Natural Sciences Foundation of China (NSFC) (grant no. 51878230 and 52178470), Natural Science Foundation of Heilongjiang Province (grant no. YQ2021E033), Postdoctoral scientific research development fund of Heilongjiang Province (grant no. LBH-Q20021), and was supported by the Department of Science and Technology of Guangdong Province (grant no. 2020B1212030001), Heilongjiang Touyan Team and Fundamental Research Funds for the Central Universities, and by field observations and research based for long-term performance of sea-crossing bridge in transportation industry.

Institutional Review Board Statement: Not applicable.

Informed Consent Statement: Not applicable.

Data Availability Statement: The data presented in this study are available on request from the corresponding author. The data are not publicly available due to privacy.

Conflicts of Interest: The authors declare no conflict of interest.

References

1. Chen, S.R.; Cai, C.S. Accident assessment of vehicles on long-span bridges in windy environments. *J. Wind. Eng. Ind. Aerodyn.* **2004**, *92*, 991–1024. [[CrossRef](#)]
2. Wang, H.; Mao, J.-X.; Spencer, B.F. A monitoring-based approach for evaluating dynamic responses of riding vehicle on long-span bridge under strong winds. *Eng. Struct.* **2019**, *189*, 35–47. [[CrossRef](#)]
3. de Oliveira, C.C.; Carvalho, H.; Verga Mendes, V.R.; Correia, J.A.F.; de Oliveira Correia, J.A.F.; Fazeres-Ferradosa, T. Nonlinear dynamic analysis of transmission line cables under synoptic wind loads. *Pract. Period. Struct. Des. Constr.* **2020**, *25*, 04020035. [[CrossRef](#)]
4. Cai, H.; Jia, X.; Feng, J.; Li, W.; Hsu, Y.-M.; Lee, J. Gaussian process regression for numerical wind speed prediction enhancement. *Renew. Energy* **2020**, *146*, 2112–2123. [[CrossRef](#)]
5. Cai, H.; Jia, X.; Feng, J.; Yang, Q.; Hsu, Y.-M.; Chen, Y.; Lee, J. A combined filtering strategy for short term and long term wind speed prediction with improved accuracy. *Renew. Energy* **2019**, *136*, 1082–1090. [[CrossRef](#)]
6. Sweeney, C.P.; Lynch, P.; Nolan, P. Reducing errors of wind speed forecasts by an optimal combination of post-processing methods: Comparing and combining post-processing methods. *Met. Apps* **2013**, *20*, 32–40. [[CrossRef](#)]
7. Torres, J.L.; García, A.; De Blas, M.; De Francisco, A. Forecast of hourly average wind speed with ARMA models in Navarre (Spain). *Sol. Energy* **2005**, *79*, 65–77. [[CrossRef](#)]
8. Kavasseri, R.G.; Seetharaman, K. Day-ahead wind speed forecasting using f-ARIMA models. *Renew. Energy* **2009**, *34*, 1388–1393. [[CrossRef](#)]
9. Chen, K.; Yu, J. Short-term wind speed prediction using an unscented kalman filter based state-space support vector regression approach. *Appl. Energy* **2014**, *113*, 690–705. [[CrossRef](#)]
10. Velo, R.; López, P.; Maseda, F. Wind speed estimation using multilayer perceptron. *Energy Convers. Manag.* **2014**, *81*, 1–9. [[CrossRef](#)]
11. Luo, X.; Sun, J.; Wang, L.; Wang, W.; Zhao, W.; Wu, J.; Wang, J.-H.; Zhang, Z. Short-term wind speed forecasting via stacked extreme learning machine with generalized coreentropy. *IEEE Trans. Ind. Inf.* **2018**, *14*, 4963–4971. [[CrossRef](#)]
12. Zhang, Z.; Qin, H.; Liu, Y.; Wang, Y.; Yao, L.; Li, Q.; Li, J.; Pei, S. Long short-term memory network based on neighborhood gates for processing complex causality in wind speed prediction. *Energy Convers. Manag.* **2019**, *192*, 37–51. [[CrossRef](#)]
13. Yu, E.; Xu, G.; Han, Y.; Li, Y. An efficient short-term wind speed prediction model based on cross-channel data integration and attention mechanisms. *Energy* **2022**, *256*, 124569. [[CrossRef](#)]
14. Yang, R.; Liu, H.; Nikitas, N.; Duan, Z.; Li, Y.; Li, Y. Short-term wind speed forecasting using deep reinforcement learning with improved multiple error correction approach. *Energy* **2022**, *239*, 122128. [[CrossRef](#)]
15. Liu, H.; Tian, H.; Li, Y. An EMD-recursive ARIMA method to predict wind speed for railway strong wind warning system. *J. Wind. Eng. Ind. Aerodyn.* **2015**, *141*, 27–38. [[CrossRef](#)]
16. Yu, C.; Li, Y.; Xiang, H.; Zhang, M. Data mining-assisted short-term wind speed forecasting by wavelet packet decomposition and elman neural network. *J. Wind. Eng. Ind. Aerodyn.* **2018**, *175*, 136–143. [[CrossRef](#)]

17. Liu, H.; Mi, X.; Li, Y.; Duan, Z.; Xu, Y. Smart wind speed deep learning based multi-step forecasting model using singular spectrum analysis, convolutional gated recurrent unit network and support vector regression. *Renew. Energy* **2019**, *143*, 842–854. [[CrossRef](#)]
18. Jiajun, H.; Chuanjin, Y.; Yongle, L.; Huoyue, X. Ultra-short term wind prediction with wavelet transform, deep belief network and ensemble learning. *Energy Convers. Manag.* **2020**, *205*, 112418. [[CrossRef](#)]
19. Hu, H.; Wang, L.; Tao, R. Wind speed forecasting based on variational mode decomposition and improved echo state network. *Renew. Energy* **2021**, *164*, 729–751. [[CrossRef](#)]
20. Qu, Z.; Mao, W.; Zhang, K.; Zhang, W.; Li, Z. Multi-step wind speed forecasting based on a hybrid decomposition technique and an improved back-propagation neural network. *Renew. Energy* **2019**, *133*, 919–929. [[CrossRef](#)]
21. Zhang, Y.; Chen, B.; Pan, G.; Zhao, Y. A novel hybrid model based on VMD-WT and PCA-BP-RBF neural network for short-term wind speed forecasting. *Energy Convers. Manag.* **2019**, *195*, 180–197. [[CrossRef](#)]
22. Sun, W.; Wang, Y. Short-term wind speed forecasting based on fast ensemble empirical mode decomposition, phase space reconstruction, sample entropy and improved back-propagation neural network. *Energy Convers. Manag.* **2018**, *157*, 1–12. [[CrossRef](#)]
23. Chen, G.; Tang, B.; Zeng, X.; Zhou, P.; Kang, P.; Long, H. Short-term wind speed forecasting based on long short-term memory and improved BP neural network. *Int. J. Electr. Power Energy Syst.* **2022**, *134*, 107365. [[CrossRef](#)]
24. Hu, J.; Heng, J.; Wen, J.; Zhao, W. Deterministic and probabilistic wind speed forecasting with de-noising-reconstruction strategy and quantile regression based algorithm. *Renew. Energy* **2020**, *162*, 1208–1226. [[CrossRef](#)]
25. Huang, X.; Wang, J.; Huang, B. Two novel hybrid linear and nonlinear models for wind speed forecasting. *Energy Convers. Manag.* **2021**, *238*, 114162. [[CrossRef](#)]
26. Peng, Z.; Peng, S.; Fu, L.; Lu, B.; Tang, J.; Wang, K.; Li, W. A novel deep learning ensemble model with data denoising for short-term wind speed forecasting. *Energy Convers. Manag.* **2020**, *207*, 112524. [[CrossRef](#)]
27. Tian, Z. Modes decomposition forecasting approach for ultra-short-term wind speed. *Appl. Soft Comput.* **2021**, *105*, 107303. [[CrossRef](#)]
28. Wang, J.; Zhang, N.; Lu, H. A novel system based on neural networks with linear combination framework for wind speed forecasting. *Energy Convers. Manag.* **2019**, *181*, 425–442. [[CrossRef](#)]
29. Qian, Z.; Pei, Y.; Zareipour, H.; Chen, N. A review and discussion of decomposition-based hybrid models for wind energy forecasting applications. *Appl. Energy* **2019**, *235*, 939–953. [[CrossRef](#)]
30. Jiang, Y.; Huang, G.; Peng, X.; Li, Y.; Yang, Q. A novel wind speed prediction method: Hybrid of correlation-aided DWT, LSSVM and GARCH. *J. Wind. Eng. Ind. Aerodyn.* **2018**, *174*, 28–38. [[CrossRef](#)]
31. Wang, Y.; Wu, L. On practical challenges of decomposition-based hybrid forecasting algorithms for wind speed and solar irradiation. *Energy* **2016**, *112*, 208–220. [[CrossRef](#)]
32. Deng, Y.; Wang, B.; Lu, Z. A hybrid model based on data preprocessing strategy and error correction system for wind speed forecasting. *Energy Convers. Manag.* **2020**, *212*, 112779. [[CrossRef](#)]
33. Liu, L.; Wang, J. Super multi-step wind speed forecasting system with training set extension and horizontal-vertical integration neural network. *Appl. Energy* **2021**, *292*, 116908. [[CrossRef](#)]
34. Wang, Y.; Wang, H.; Srinivasan, D.; Hu, Q. Robust functional regression for wind speed forecasting based on Sparse Bayesian learning. *Renew. Energy* **2019**, *132*, 43–60. [[CrossRef](#)]
35. Yang, W.; Tian, Z.; Hao, Y. A novel ensemble model based on artificial intelligence and mixed-frequency techniques for wind speed forecasting. *Energy Convers. Manag.* **2022**, *252*, 115086. [[CrossRef](#)]
36. Duarte, F.S.L.G.; Rios, R.A.; Hruschka, E.R.; de Mello, R.F. Decomposing time series into deterministic and stochastic influences: A survey. *Digit. Signal Process.* **2019**, *95*, 102582. [[CrossRef](#)]
37. Vautard, R.; Yiou, P.; Ghil, M. Singular-spectrum analysis: A toolkit for short, noisy chaotic signals. *Phys. D Nonlinear Phenom.* **1992**, *58*, 95–126. [[CrossRef](#)]
38. Golyandina, N.; Zhigljavsky, A. *Singular Spectrum Analysis for Time Series*; SpringerBriefs in Statistics; Springer: Berlin/Heidelberg, Germany, 2020; ISBN 978-3-662-62435-7.
39. Leles, M.C.R.; Sansão, J.P.H.; Mozelli, L.A.; Guimarães, H.N. Improving reconstruction of time-series based in singular spectrum analysis: A segmentation approach. *Digit. Signal Process.* **2018**, *77*, 63–76. [[CrossRef](#)]
40. Chung, J.; Gulcehre, C.; Cho, K.; Bengio, Y. Empirical evaluation of gated recurrent neural networks on sequence modeling. *arXiv* **2014**, arXiv:1412.3555.
41. Graves, A.; Jaitly, N. Towards end-to-end speech recognition with recurrent neural networks. In Proceedings of the 31st International Conference on Machine Learning, Beijing, China, 21–26 June 2014; p. 9.
42. Wei, D.; Wang, J.; Niu, X.; Li, Z. Wind speed forecasting system based on gated recurrent units and convolutional spiking neural networks. *Appl. Energy* **2021**, *292*, 116842. [[CrossRef](#)]
43. Xiong, D.; Fu, W.; Wang, K.; Fang, P.; Chen, T.; Zou, F. A blended approach incorporating TVFEMD, PSR, NNCT-based multi-model fusion and hierarchy-based merged optimization algorithm for multi-step wind speed prediction. *Energy Convers. Manag.* **2021**, *230*, 113680. [[CrossRef](#)]
44. Huang, G.-B.; Zhou, H.; Ding, X.; Zhang, R. Extreme learning machine for regression and multiclass classification. *IEEE Trans. Syst. Man Cybern. B* **2012**, *42*, 513–529. [[CrossRef](#)] [[PubMed](#)]
45. Huang, G.-B.; Wang, D.H.; Lan, Y. Extreme learning machines: A survey. *Int. J. Mach. Learn. Cyber.* **2011**, *2*, 107–122. [[CrossRef](#)]
46. Huang, G.-B.; Zhu, Q.-Y.; Siew, C.-K. Extreme learning machine: Theory and applications. *Neurocomputing* **2006**, *70*, 489–501. [[CrossRef](#)]

-
47. He, K.; Zhang, X.; Ren, S.; Sun, J. Deep residual learning for image recognition. In Proceedings of the 2016 IEEE Conference on Computer Vision and Pattern Recognition (CVPR), Las Vegas, NV, USA, 30 June 2016; pp. 770–778.
 48. Krizhevsky, A.; Sutskever, I.; Hinton, G.E. ImageNet classification with deep convolutional neural networks. *Commun. ACM* **2017**, *60*, 84–90. [[CrossRef](#)]